Catal Lett (2016) 146:433–441
DOI 10.1007/s10562-015-1649-6

Effect of Ni Loading on Lanthanide (La and Ce) Promoted γ-Al_2O_3 Catalysts Applied to Ethanol Steam Reforming

Cristian H. Campos[1] · Paula Osorio-Vargas[2] · Nicolás Flores-González[2] · Jose L. G. Fierro[3] · Patricio Reyes[2]

Received: 28 July 2015 / Accepted: 3 November 2015 / Published online: 28 November 2015

Abstract Hydrogen production from ethanol steam reforming over xNi/15 %La_2O_3–10 %CeO_2–γ-Al_2O_3 (x = 5, 10 and 15 wt %) catalysts was investigated with an ethanol:water = 1:3 feed composition. The results of catalysts characterization suggest that Ni metal particles have a strong metal support interaction with the promoters on the surface. Ethanol was completely converted to hydrogen and C_1 products (CO, CO_2, CH_4) even at 723 K due to the remarkable C–C bond cleavage capacity and resistance to coke formation conferred by the promoters at low metal loadings. The increase of Ni particle size decreases the stability and selectivity; catalyst deactivation during 24 h on stream was attributed to coke deposition.

Graphical Abstract

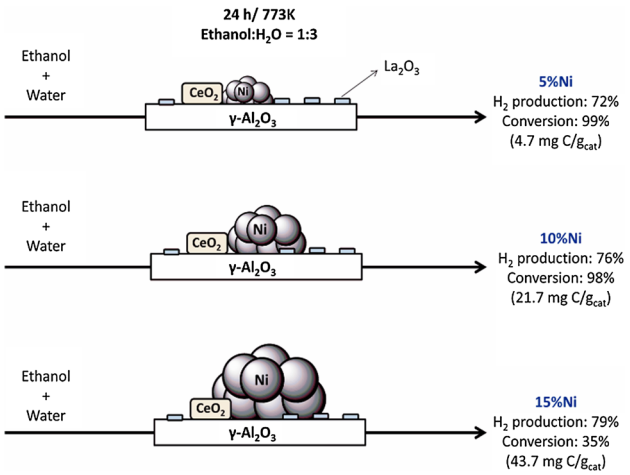

Keywords Lanthanide promoters · Steam reforming · Hydrogen production · Catalyst stability

1 Introduction

Hydrogen is potentially a very attractive source of clean energy since its combustion produces only water and energy. In that regard, ethanol is a very flexible resource for the production of hydrogen since it can be derived from several biomass sources. In addition, it is relatively inexpensive and possesses a high H_2 production capacity per molecule of ethanol reformed [1–4]. A wide range of catalysts have been tested for bio-ethanol catalytic steam reforming, changing both the active phase (Rh, Pt, Pd, Ru, Ni, Cu, Zn, Fe) and the support (Al_2O_3, 12 %CeO_2–Al_2O_3, CeO_2, CeO_2–ZrO_2,

✉ Cristian H. Campos
ccampos@udec.cl

[1] Departamento de Química Orgánica, Facultad de Ciencias Químicas, Universidad de Concepción, Edmundo Larenas 129, Concepción, Chile

[2] Departamento de Físico-Química, Facultad de Ciencias Químicas, Universidad de Concepción, Edmundo Larenas 129, Concepción, Chile

[3] Instituto de Catálisis y Petroleoquímica (CSIC), C/Marie Curie 2, Cantoblanco, 28049 Madrid, Spain

ZrO_2). At 973 K and atmospheric pressure, γ-Al_2O_3-supported Rh and Ni gave the best performance compared to Pt, Cu, Zn or Fe [5, 6]. Among transition metals, Ni has been widely used as active phase for ethanol-reforming reactions because of its high C–C and O–H bond-breaking activity [7–9], its relatively low cost and its known participation in the WGS reaction [10]. Alumina, which is widely used as a support, exacerbates catalyst deactivation by deposition of carbon from the ethylene intermediate produced via dehydration reactions of ethanol on acid sites of the support. For that reason, γ-Al_2O_3 has typically been modified by addition of alkali metals, rare earth oxides and other basic oxides to decrease the acidity, enhance the oxygen mobility, improve the metal dispersion and prevent the sintering of metal sites [5, 7]. Supported by experimental and density-functional theory (DFT) studies, the effect of the support on Ni stability not always showed an enhancement of Ni on the supports surface. At the origin of the support effect is the ability of metal oxides to stabilize oxidized Ni^{2+} species by accommodating electrons in localized f-states [11–15] which are responsible for activating the H_2O molecule.

Among modifiers, La_2O_3 has been used as support promoter for enhancing the stability of Ni-based catalysts, which is attributed to scavenging of carbonaceous species from coke deposition by lanthanum oxycarbonate species that are developed on the top of Ni particles or at the Ni–La interface [16, 17]. Likewise, CeO_2 has also shown excellent results in catalyst stability as it favours the gasification of coke and the WGS reaction due to its capacity to store, release and transport oxygen. Recently, theoretical results have corroborated the experimental observations that CeO_2 stabilizes oxidized Ni species by accommodating electrons in localized f-states, and Ni adatoms (Ni^{2+}) are markedly different from larger 3D Ni particles or metallic Ni (Ni^0). On the other hand, it has been reported that CeO_2 improves the redox reversibility of the metallic phase and prevents the loss of surface area of bare alumina and the sintering of the metallic species during the thermal treatment [18–20].

The aim of this paper is to study the effect of Ni loading of rare-earth-doped γ-Al_2O_3 supported catalysts on the stability and selectivity of the ESR reaction. γ-Al_2O_3 support was modified with both CeO_2 and La_2O_3 promoters in order to improve the Ni surface stability (conversion and H_2 production) during the ESR at 723 K according to previous results [21–25].

2 Experimental

2.1 Catalyst Preparation

The supports were prepared by successive wet impregnation of inorganic precursors of La_2O_3 and CeO_2 (in the order: La_2O_3–$x$$CeO_2$–γ-$Al_2O_3$) on γ-$Al_2O_3$ (Glider S_{BET} = 189 m^2/g): an appropriate amount of aqueous solution of $Ce(NO_3)_3{\cdot}6H_2O$ and $La(NO_3)_3{\cdot}6H_2O$ was added to γ-Al_2O_3 under stirring for 4 h at room temperature, to obtain catalysts containing 15 wt % La_2O_3–10 wt % CeO_2–Al_2O_3. After every impregnation, the support was dried at 373 K for 0.5 h and finally calcined at 923 K for 6 h under static air. The supported Ni catalysts were prepared by impregnation with aqueous solutions of nickel nitrate ($Ni(NO_3)_2{\cdot}6H_2O$),S following the aforementioned procedure, to obtain catalysts with 5, 10 and 15 wt % Ni on 15 wt %La_2O_3–10 wt %CeO_2–γAl_2O_3 (5, 10 and 15Ni/LCA). The samples were calcined under dynamic air (30 mL min^{-1}) at 773 K for 4 h at a heating rate of 10 K min^{-1}. The solids were reduced prior to characterization or catalytic evaluation in H_2 flow (30 mL min^{-1}) at 923 K for 1.5 h.

2.2 Catalyst Characterization

The metal content was analyzed by an inductively coupled plasma (ICP) atomic emission spectrometer (PLASMA-SPEC-II). The BET specific surface areas (S_{BET}) and pore volumes of the samples were determined using an automatic Micromeritics apparatus Model ASAP 2010 instrument. Temperature–programmed reduction (TPR) was measured in a semiautomatic Micromeritics TPD/TPR 2900 apparatus equipped with a TCD [26]. X-ray diffraction (XRD) patterns were recorded on a Bruker diffractometer Model D4 Endeavor equipped with a Cu K_α radiation source under constant operation at 40 kV and 100 mA. TEM images were obtained in a JEOL Model JEM-1200 EXII microscope operating at 300 kV. Samples were prepared by ultrasonically suspending the sample in ethanol and depositing a drop of the suspension onto a copper grid. X-ray photoelectron spectra (XPS) of reduced catalysts prior to the reaction were recorded on a VG Escalab 200R electron spectrometer. Details of the experimental procedure have been reported in a previous work [26]. The quantity of coke deposited on the spent catalysts was determined by temperature-programmed oxidation (TPO) by thermogravimetry (TGA/SDTA851 Mettler Toledo), measuring the mass loss of the spent catalysts during oxidation.

2.3 Catalytic Evaluation in the Steam Reforming of Ethanol

Activity tests were performed using 100 mg of catalyst diluted with 200 mg of SiC (both materials were in the 0.18–0.36 mm particle size range which was selected after preliminary mass transport experiments to minimize diffusional resistances) to avoid adverse thermal effects. The

catalyst bed was placed in a 1.7 cm ID stainless steel tubular reactor with a coaxially centered thermocouple. Prior to the reaction, the catalysts were heated in Ar flow (33 mL min^{-1}) up to 773 K (10 K min^{-1}), followed by reduction in situ at 773 K for 1.5 h with H_2 flow (30 mL min^{-1}), and subsequently by a purge with Ar flow (33 mL min^{-1}) for 1 h. The mixture water/ethanol (3/1 mol ratio) was fed from a liquid phase by a HPLC pump (Gilson 307) with a flow of 0.09 mL min^{-1} and then it was carried to the reactor by Ar with a total flow of 137 mL min^{-1} (molar ratio $Ar/(H_2O + EtOH) = r.d = 0.76$) under a GHSV = 26,000 h^{-1} at atmospheric pressure. The catalytic activity was measured at 773 K for 24 h of time on stream in order to study the catalyst stability. The reaction products were monitored using a quadrupole mass spectrometer (Hiden Model HPR-20) connected on line to the reactor through a heated capillary tube. The transient-MS signals at m/z = 2, 15, 18, 26, 28, 29, 30, 31, 44 and 58 were continuously recorded for H_2, CH_4, H_2O, C_2H_4, CO, C_2H_4O, C_2H_6, C_2H_5OH, CO_2 and C_3H_6O respectively. The intensity of each product was represented by the selected signal after subtracting the possible contributions of fragments from other compounds. Such contributions were calculated on the basis of the intensity ratios between the fragments characteristic of the individual molecules. Ethanol conversion and selectivity were calculated from the following equations.

$$\text{Conversion} : X(\%) = \frac{n_{Ethanol,in} - n_{Ethanol,out}}{n_{Ethanol,in}} \cdot 100$$

$$\text{Selectivity} : S(\%) = \frac{n_i}{\sum_n n_i} \cdot 100$$

where n_i is the number of moles of product i, $n_{ethanol}$ is the moles number of ethanol.

The quantity of coke deposited on the spent catalysts was determined by temperature-programmed oxidation (TPO) by thermogravimetry (TGA/SDTA851 Mettler Toledo), measuring the mass loss of the spent catalysts during oxidation. Each sample was previously heated up to 773 K for 1 h in N_2 (10 K min^{-1}, 200 mL min^{-1}) to remove volatile compounds adsorbed on the catalyst surfaces. TPO was performed from 303 K (5 K min^{-1}) until a final temperature of 1273 K under flow of 20 vol % O_2 in N_2. Quantification of coke deposited on catalysts was calculated according to the equation:

$$C = \frac{m_{coke}}{m_{used\ catalyst} \times t}$$

where m_{coke} is the mass of coke deposited on the catalyst, calculated from TPO-TGA, $m_{used\ catalyst}$ is the mass of catalyst calculated from the mass remaining after the TG analysis, and t is the time under reaction.

The nature and characteristics of carbon deposits were also studied by Raman spectroscopy. Raman spectra were recorded with a Renishaw in via Raman microscope spectrometer equipped with a laser beam emitting at 532 nm, at 100 mW output power. Each spectrum acquisition consisted of 5 accumulations of 5 s, collected at room temperature.

3 Results and Discussion

3.1 Characterization of Supports and Fresh Catalysts

Alumina is one of the most widely used catalyst supports, and hence a study of its promotion with La_2O_3 and CeO_2 for ESR at different Ni loadings is of interest. The optimal quantity of La_2O_3 (15 wt %) doped in 10 %Ni/Al_2O_3 catalyst in the ESR at low temperatures has been reported by Fierro et al. [26]. We probed the addition of a second promoter, CeO_2 at 10 wt %, to improve the stability of the catalysts by enhancing the electronic interactions between nickel species and La_2O_3-CeO_2 oxides added to the support [25, 27, 28]. During the γ-Al_2O_3 modification, the addition of CeO_2 and La_2O_3 was carried out by successive wet impregnation, first with Ce followed by La, because this methodology enhances the dispersion of both promoters on the support surface.

ICP analysis revealed that the Ni loadings in the prepared catalysts were 4.97, 9.98 and 14.91 wt %, respectively, as shown in Table 1. Ce and La contents are very close to the nominal values and showed similar content after the Ni impregnation. The specific surface area (S_{BET}) and pore volume (V_p) of γ-Al_2O_3 progressively decreases by modification of the support with both promoters (La_2O_3 and CeO_2) and the impregnation of different Ni amounts, indicating that these species produced changes in the textural properties of the alumina support as shown in Table 1. A possible explanation for the loss of surface area is that the high loadings may have increased the coverage of the γ-Al_2O_3 pore walls with oxide species (CeO_2, La_2O_3) and Ni nanoparticles.

The XRD patterns of the reduced catalysts are shown in Fig. 1. All the catalysts showed diffraction peaks at approximately $2\theta = 37.2°$, 45.8° and 66.7°, which correspond to γ-Al_2O_3 (JCPDS 86-1410). The peaks observed at 2θ of 28.60, 33.1, 47.6, and 56.5° were respectively indexed as (1 1 1), (2 0 0), (2 2 0), and (3 1 1) planes of the fluorite structure (JCPDS 081-0792) of CeO_2, which suggests the segregation of the CeO_2-phase over the γ-Al_2O_3 surface. No diffraction peaks corresponding to crystalline species of either La_2O_3 (JCPDS 83-1355) or $LaAlO_3$

Table 1 Metal contents from ICP-AES, textural properties of supports/catalysts obtained from N_2 isotherms at 77 K

Support	Ni content (wt %)	Ce content (wt %)	La content (wt %)	$S_{BET}(m^2\ g^{-1})$	$V_{pore}\ (cm^3\ g^{-1})^a$
A	–	–	–	189	0.36
CA	–	9.8	–	154	0.31
LCA	–	6.8	14.7	111	0.28
5 %Ni/LCA	4.9	6.3	13.0	120	0.25
10 %Ni/LCA	9.9	6.1	12.1	99	0.21
15 %Ni/LCA	14.8	5.7	11.4	80	0.17

A γ-Al_2O_3, *CA* 10 %CeO_2-Al_2O_3, *LCA* 15 %La_2O_3-10 %CeO_2-Al_2O_3

[a] Pore volume calculated from the desorption branch of the N_2 physisorption isotherm

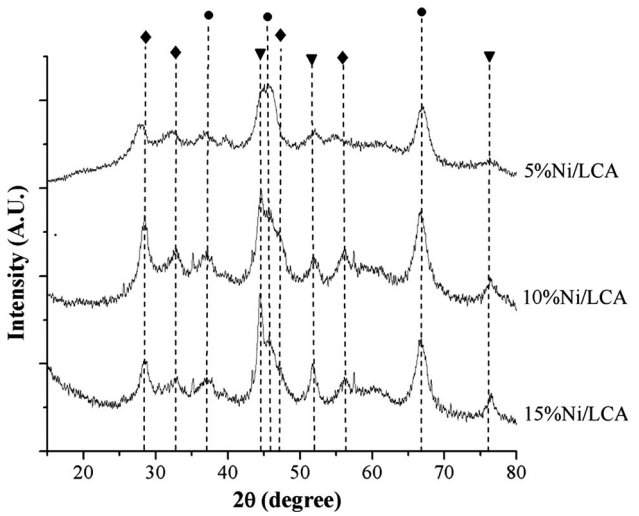

Fig. 1 X-ray diffraction patterns of the reduced catalysts. Ni^0(*black down pointing triangle*), (*filled circle*) γ-Al_2O_3, (*filled diamond*) CeO_2

(JCPDS 85-1071) were observed in the catalysts [29–31]. Three major peaks attributed to Ni° (1 1 1) at 44.5°; Ni°(2 0 0) at 51.8° and Ni°(2 2 0) at 76.5° were detected in all of the catalysts.

As shown in Fig. 1, the increase in the metal loadings generates changes in the intensity of Ni diffraction patterns attributed to the changes in the metallic particle size distribution. There is no evidence of NiO (37.3°, 43.3° and 62.9° JCPDS 78-0643) in the XRD patterns of the studied catalysts indicating that the nickel present on the support is in the metallic form or a highly dispersed non-stoichiometric amorphous nickel aluminate spinels species as was observed in previous reports [17, 23, 32–34]. The diffraction peaks attributable to $NiAl_2O_4$ appear at 19.1°, 31.4°, 37.0°, 45.0° and 65.5° (JCPDS 10-339), although it is difficult to distinguish the diffraction peaks of $NiAl_2O_4$ or mixed oxides (substitution of Al and Ni by Ce and La in $NiAl_2O_4$ spinels) in the Ni/LCA catalysts from those of γ-Al_2O_3 and CeO_2 due to its broad diffraction signals.

Figure 2 shows the HR-TEM micrographs of the reduced catalysts. Clearly, spherical Ni particles are incorporated in the CeO_2–La_2O_3 modified supports (Fig. 2a–c). The 5Ni/LCA catalysts prepared by the impregnation method had nano-sized (~7.8 nm) nickel particles, showing a better nickel dispersion than 10Ni/LCA (~8.4 nm) and 15Ni/LCA (~12.1 nm).

Figure 3 shows the H_2-TPR profiles for the prepared catalysts. TPR data showed differences in the relative proportion of nickel species depending on metal loading used and the reduction profiles of catalysts consist of a broad peak ranging from 475 to 1100 K and reveals different degrees of interaction of nickel species with the support. The TPR of NiO/γ-Al_2O_3 system under hydrogen atmosphere has been thoroughly discussed in several previous studies [35–38]. For our catalysts, the reduction peak at lower temperatures, 550 and 650 K, are related to the reduction of highly dispersed amorphous NiO with a strong interaction with the promoters on the support [34, 39, 40]. Hydrogen consumption peaks of Ni/Al_2O_3 catalyst have been ascribed to the reduction of amorphous Ni mixed oxides or highly dispersed non-stoichiometric amorphous nickel aluminate spinels at temperatures close to 770 K [32, 41]. For our Ni catalysts, however, the reduction temperature of Ni species shifts to 670 K as a consequence of the incorporation of Ni ions into the mixed metal oxide matrix. For 10Ni/LCA and 15Ni/LCA catalysts a decrease in the proportion of diluted $NiAl_2O_4$ (peak up to 860 K) can also be observed, increasing the contribution of the highly dispersed non stoichiometric amorphous nickel aluminate phase (peak at 750 K, Fig. 3), as can also be observed by comparing the reduction profile of 5Ni/LCA sample with the reduction profiles of 10Ni/LCA and 15Ni/LCA samples.

This is in good agreement with results reported by Zhang et al. [38] that $NiAl_2O_4$ was the major species formed at low Ni loading. At lower Ni loading, the metal precursor is in intimate contact with the doped-support which could promote the formation of non-stoichiometric

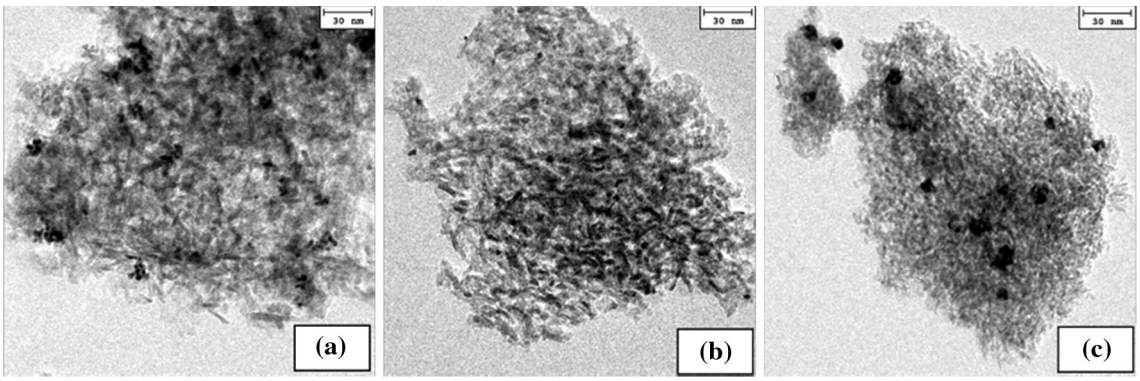

Fig. 2 TEM micrographs of reduced catalysts: **a** 5 %Ni/LCA, **b** 10 %Ni/LCA, **c** 15 %Ni/LCA

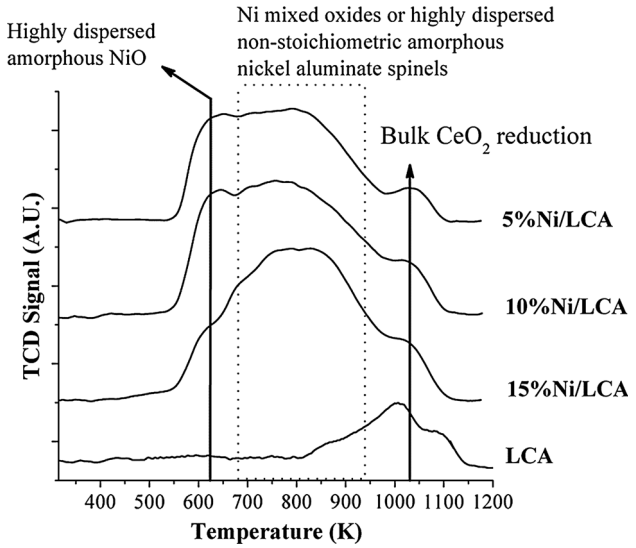

Fig. 3 H2-TPR profiles of the Ni supported catalysts

amorphous nickel aluminate spinels. On the other hand, Ni particles avoid excessive growth at high temperature which could enhance the catalytic performance and provide better stability. Finally, additional less pronounced peaks at 380 and 490 K as can be seen, which could be ascribed to the reduction of isolated CeO_2 species (not detected by XRD) while the bulk CeO_2 species (detected by XRD) are maintained after the reduction process at 1030 K as can see in Fig. 3 [40].

The reduced Ni catalysts were analyzed by XPS to study the oxidation state and surface compositions and results are summarized in Table 2. The binding energy (BE) of La $3d_{5/2}$ was observed between 834.7 and 835.0 eV and was substantially higher than the values reported for La_2O_3 (833.2 eV) and $LaAlO_3$ (833.8 eV) standards. However, these values have already been reported by some authors [26, 42, 43] and have been attributed to deficiently coordinated La^{3+} ions. In addition, the calculated La/Al atomic ratio (Table 2) higher than the values corresponding to the bulk composition is indicative of diffusion at surface level of lanthanum ions into the alumina framework in all cases. For the Ce $3d_{5/2}$ level, a BE of 883.0 eV characteristic of CeO_2 was determined, showing that no detectable Ce^{+3} was present. The Ni $2p_{3/2}$ core-levels (Table 2) were deconvoluted into two contributions, at binding energies of 851.0–851.6 and 854.7–855.2 eV, which have been assigned to Ni^0 and Ni^{2+}, respectively. Binding energies for Ni^0 $2p_{3/2}$ are shifted with respect to those of the bulk atoms (852.6 eV), as a consequence of differences in charge density between different atoms. The surface atoms acquire a negative charge relative to the bulk, by SMSI, and consequently the surface core levels shift to lower binding energy [44, 45]. On the other hand, the existence of

Table 2 HR-TEM particles diameter, binding energies (eV) and atomic surface ratio from XPS analyses of reduced Ni supported catalysts

Catalyst	$d_{HR\text{-}TEM}$ (nm)	Ce $3d_{5/2}$ (eV)	La $3d_{5/2}$ (eV)	Ni $2p^a_{3/2}$ (eV)		Ce/Al^b_{at}	La/Al^b_{at}	$Ni/(Ce + La + Al)^b_{at}$
				Ni^0	Ni^{2+}			
5 %Ni/LCA	7.8 ± 3.1	883.0	835.1	851.8 (27)	855.2 (73)	0.022 (0.033)	0.192 (0.061)	0.133 (0.055)
10 %Ni/LCA	8.4 ± 3.8	883.0	835.0	851.6 (41)	854.8 (59)	0.024 (0.033)	0.152 (0.061)	0.293 (0.115)
15 %Ni/LCA	12.1 ± 4.9	883.0	835.1	851.6 (30)	855.2 (70)	0.026 (0.033)	0.253 (0.061)	0.551 (0.183)

[a] Percentage in brackets

[b] Nominal value in brackets

both species (Ni° and Ni^{2+}) point out that the reduction procedure used did not lead to a complete reduction, probably due to Ni^{2+} species strongly interacting with the support as was suggested by XRD and TPR results. As summarized in Table 2, the proportion of nickel in the metallic state was lower than the Ni^{2+} in all cases and the 10 %Ni/LCA catalyst exhibits a higher $Ni°/Ni^{2+}$ ratio.

As the nickel loading increased from 5.0 to 15.0 wt %, the main peak at BE = 851.6 eV displays an increase in the contribution for metallic Ni (see Table 2). Charge transfer from the support to the particle, especially in systems with metallic particles on reducible metal oxides, can alter the electronic properties of the particles [46, 47].

3.2 Catalytic Evaluation and Selectivity Stability for the Steam Reforming of Ethanol

Figure 4 compares the temperature-dependence of ethanol conversion and product selectivity during ethanol steam reforming over the Ni/LCA catalysts. At 773 K all catalysts attained complete conversion and remained stable until 923 K. On the 5 %Ni/LCA catalyst, CH_4, CO and CH_3CHO were formed as major by-products at 723 K. This product distribution indicates that ethanol dehydrogenation and decomposition were the primary reactions [26, 48]. At temperatures higher than 773 K, acetaldehyde was mostly converted into H_2, and CH_4. As temperature is further increased, the selectivity toward CO and CO_2 slightly increased while the selectivities to CH_4 decreased. This indicates that the methane steam reforming (MSR), which is thermodynamically feasible at high temperatures, was the predominant reaction upon reaching 773 K. At 923 K, the outlet gases consisted of 76 % H_2, 13 % CO, 8 % CO_2 and 3.8 % CH_4. At high temperatures, MSR and the reverse WGS are predominant reactions, producing an increase in the CO selectivity [49]. In our system, as was discussed in the characterization section, 5 %Ni/LCA catalyst showed a lower contribution of Ni^0 species on the surface (see Table 2). Ganduglia-Pirovano reported experimental/theoretical evidence for the Ni/CeO_2 catalyst in the WGS reaction where at low Ni loading, Ni is present as Ni^{2+} mainly, as a consequence of the Ni ↔ CeO_2 surface interactions [46]. This SMSI provides an easier dissociation of O–H bonds from H_2O and makes it difficult to cleave C–O bonds during WGS reaction. In our case, the presence of both La_2O_3 and CeO_2 promoters in the catalyst surface increased SMSI effect and promoted the H_2O activation in MSR. Finally, under these conditions, the WGS reaction also approached its equilibrium at 923 K.

The 10 %Ni/LCA catalyst only displayed a traceable amount of CH_3CHO; the major reaction was the decomposition of ethanol and CH_3CHO to CH_4, CO_2 and CO. This indicated that 10 %Ni/LCA catalyst showed a stronger capacity for breaking the C–C bond in ethanol. Therefore, the reaction pathway of ESR at lower temperatures is strongly dependent on the capacity of the Ni particles for breaking the C–C bond in the ethanol molecule. At higher temperatures, significant increases in CO concentration together with

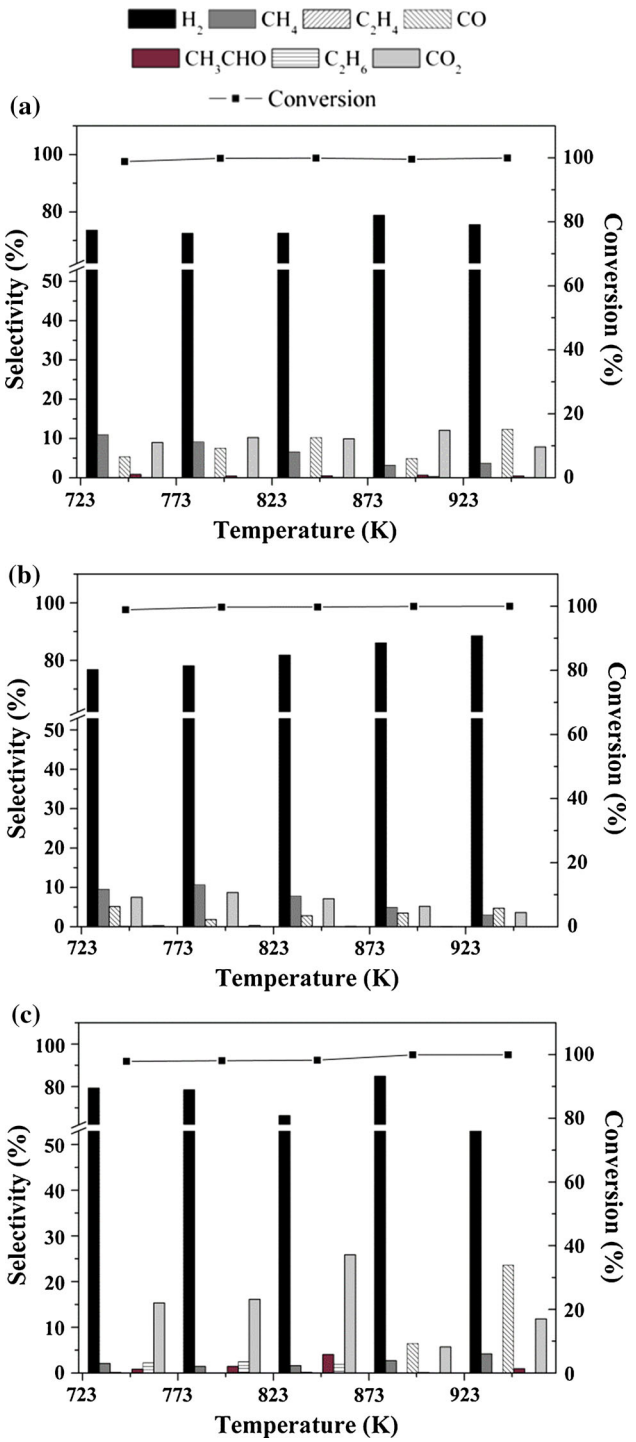

Fig. 4 Effect of reaction temperature on the products distribution in the outlet dry stream of ESR over xNi/LCA catalysts. Experimental conditions: 723–923 K; catalyst: 100 mg; H_2O:EtOH = 3:1; GHSV = 27000 h^{-1}. **a** 5 %Ni/LCA, **b** 10 %Ni/LCA and **c** 15 %Ni/LCA

Table 3 ESR at 773 K under stoichiometric reaction conditions (H_2O:EtOH = 3:1) at atmospheric pressure on xNi/LCA catalysts

Catalysts	Time (h)	mol_{H_2}/mol_{EtOH}	Selectivity (mol%)							Conversion %	Reference
			H_2	CH_4	CO	CO_2	CH_3CHO	Ethylene	Ethane		
10 %Ni/Al_2O_3	2	5.7	81	4.9	0.7	5.5	0.53	5.3	1.6	99	[25]
	24	4.0	28	5.7	0	8.3	22	24	0	49	
10 %Ni/LA[a]	2	5.6	80	11	3.2	19	0.16	0.91	0.11	100	[25]
	24	4.6	58	14	7.0	10	0.67	0	0	89	
10 %Ni/CA[b]	2	5.6	60	18	7.5	22	–	5.0	–	100	[28]
	24	4.7	56	5.0	7.5	20	–	18	–	96	
5 %Ni/LCA	2	5.1	72	9.2	7.5	10	0.44	0.10	0.34	100	This work
	24	5.1	72	3.9	12	10	1.8	0.10	0.2	99	
10 %Ni/LCA	2	5.5	78	11	1.9	8.7	0	0.11	0.33	100	This work
	24	5.4	76	8.9	3.9	10	0.36	0.47	0	98	
15 %Ni/LCA	2	5.6	79	1.5	0	16	1.2	0.23	2.5	98	This work
	24	2.5	35	6.2	5.3	38	11.2	1.4	2.6	71	

[a] Prepared at 15 wt%La_2O_3

[b] Prepared at 10 wt% CeO_2 both follow the same supports preparations reported in this work. CH_3CHO and ethane selectivity were not reported

decreasing concentrations of CH_4 and CO_2 were observed, suggesting that the MSR and the reverse WGS reaction occurred as major reactions. At 923 K, the outlet gas contained 88 % H_2, 5 % CO, 4 % CO_2 and 3 % CH_4. The lower CH_4 selectivity and the higher H_2 yield demonstrated an enhanced activity for the MSR with this catalyst.

In comparision with previous results for 10 %Ni/Al_2O_3 catalysts (see Table 3) and then independently modified with CeO_2 and La_2O_3 promoters, the 10Ni/LCA catalyst showed a significant enhancement in the selectivity stability, in function of time-on-stream, during ESR [25, 26, 28]. Ni catalyst supported on bare Al_2O_3 and on modified Al_2O_3 with 10 wt % CeO_2 showed the highest selectivity to ethylene (24 and 18 %, respectively) at 24 h on-stream. The highest selectivity to ethylene with these two catalysts indicates that at this temperature (773 K) the dehydration of ethanol is favoured on this type of catalyst. On the other hand, 10 %Ni/Al_2O_3 catalyst with 15 wt% La_2O_3 catalyst exhibited a completely different selectivity compared to the modified catalysts. The selectivity followed the order: $H_2 \gg CH_4 > CO_2 > CO \gg$ acetaldehyde $\approx$ ethylene $\approx$ ethane. The presence of both promoters (CeO_2 and La_2O_3) in the support greatly improved the catalytic activity of the catalysts in the ESR reaction at 773 K by lanthanum-oxicarbonate species and O-mobility/H_2O activation as a result of CeO_2 on the support surface.

A different reaction pattern was observed with the 15 %Ni/LCA catalyst where the H_2 yield readily approached almost 80 % at about 773 K, which is similar to that of 5 %Ni/LCA and 10 %Ni/LCA catalysts. Upon heating, H_2 concentration progressively decreased together with a significant increase in CO_2 until 823 K due to MSR. At higher temperature (873–923 K), an appreciable increase in the reverse WGS reaction promoted an increase in the selectivity to CO with a simultaneous decrease of H_2 and CO_2. At 923 K, the outlet dry gas consisted of 60 mol % H_2, 24 mol % CO, 12 % CO_2 and 4 mol % CH_4. The higher CO selectivity demonstrated enhanced activity of Ni-based catalysts for C–O bond activation. The rare-earth metal oxide effect, specially CeO_2, on the Ni particles stabilizes oxidized Ni species by accommodating electrons in localized f-states, and thus the Ni atoms (Ni^{2+}) are markedly different from larger 3D Ni particles or metallic Ni (Ni^0) [50–52]. As Ni surface content increases, the SMSI effect decreases, promoting the effect of larger Ni^0 on the CO_2 activation during the reverse WGS reaction, in agreement with theoretical studies [12, 45, 46].

The development of stable catalysts is one of the most important issues in ESR at longer time-on-stream; Table 3 displays the molar concentrations of H_2, CO_2, CH_4, CO and other products in the outlet dry gas at 2 and 24 h on stream operation over the Ni/LCA catalysts at 773 K. The presence of lanthanum oxycarbonate formations from La_2O_3 promoter and the higher amount of mobile lattice oxygen induced by the CeO_2 promoter plays an important rolewith regards to increase in carbon gasification [26, 48]. It can be seen that the concentrations of the products over the 5 %Ni/LCA and 10 %Ni/LCA catalyst were stable during the initial 24 h on-stream. The conversion of ethanol only decreased slightly from 100 to 99 % at 24 h. Meanwhile, the concentrations of H_2, CO, CO_2 and CH_4 in the outlet gas varied slightly over the whole run. Despite the stability of the catalysts at these metal loadings, the amount of carbon deposited on the 5 %Ni/LCA catalyst was 4.7 mg C/g, which is much lower than that of the 10 %Ni/LCA catalyst (21.7 mg C/g). The increase in the average

Ni particle size promotes the production of CO_2 as indicated by deposition of coke. It is apparent that the 5 %Ni/LCA catalyst is characterized by less coke deposition because of its enhanced ability to activate water. The incorporation of CeO_2-La_2O_3 into the lattice of γ-Al_2O_3 created large amounts of surface defects that allowed for efficient H_2O activation and a fast diffusion of the adsorbed intermediates to the metal particles at the Ni–(Ce–La) interface where the reaction occurs. The promoters enhance the ability of Ni particles to break the C–C bond of ethanol and the facile activation of water on the support avoids carbon accumulation on the catalyst surface.

Over the 15 %Ni/LCA catalyst that was used for 24 h, the significant production of CO_2 at 773 K indicated heavy deposition of coke. The small Ni nanoparticles tended to aggregate into larger particles at higher Ni loading (see Table 2). The increase in the Ni particles size provided insufficient Ni-promoter interfacial perimeter, which resulted in significant deactivation during the ESR reaction. Therefore, it can be suggested that the decrease of conversion levels and H_2 selectivity can be attributed to catalyst desactivation and the sintering of metal particles even for 24 h on stream.

4 Conclusions

CeO_2-La_2O_3 promoted γ-Al_2O_3 supported Ni catalysts, at different metal loadings, were significantly active and selective for hydrogen production by steam reforming of ethanol with a stoichiometric feed composition. Full ethanol conversion was achieved even at 723 K with H_2 and C_1 products as the major products ($CO + CO_2 + CH_4 \leq 20$ %). Steam reforming of methane and reverse water gas shift were the major reactions which determined the outlet gas composition at higher temperatures. More importantly, the Ni/LCA catalysts showed a dependence on the Ni particles size in the catalytic performance for 24 h time-on-stream. The strong interaction between Ni and CeO_2–La_2O_3 greatly promotes the redox property of the Ni by surface oxygen vacancies. Sufficient H_2O activation accelerates the reaction rate of the intermediates and also eliminates the probable carbonaceous deposits by a strong Ni-oxide interaction. In addition, lower Ni loadings enhance the thermal stability of the catalyst at higher temperatures and partially prevent the coke deposition at 24 h-on-stream.

Acknowledgments Authors thank CONICYT for financial support FONDECYT postdoctoral GRANT 3140130 and P. Osorio-Vargas thanks to Red Doctoral REDOC, MINEDUC Project UCO 1202 and CTA MECESUP for doctoral fellowship. Nicolás A. Flores thanks Fondo Tesis CCTE-UDT for fellowship.

References

1. Bshish A, Yaakob Z, Narayanan B, Ramakrishnan R, Ebshish A (2011) Chem Pap 65:251–266
2. Contreras JL, Salmones J, Colín-Luna JA, Nuño L, Quintana B, Córdova I, Zeifert B, Tapia C, Fuentes GA (2014) Int. J. Hydrog Energy 39:18835–18853
3. Haryanto A, Fernando S, Murali N, Adhikari S (2005) Energy Fuels 19:2098–2106
4. Zanchet D, Santos JBO, Damyanova S, Gallo JMR, Bueno JMC (2015) ACS Catal. 5:3841–3863
5. Auprêtre F, Descorme C, Duprez D (2002) Catal. Comm. 3:263–267
6. Turczyniak S, Machocki A (2014) Przem Chem 93:1850–1854
7. Ni M, Leung DYC, Leung MKH (2007) Int J Hydrog Energy 32:3238–3247
8. Wu HJ, La Parola V, Pantaleo G, Puleo F, Venezia AM, Liotta LF (2013) Catalysts 3:563–583
9. Youn MH, Seo JG, Jung JC, Chung JS, Song IK (2010) Catal Surv Asia 14:55–63
10. Kugai J, Velu S, Song C (2005) Catal Lett 101:255–264
11. Bell AT, Li WD, Li YW, Qin ZF, Chen SY (1994) Chem Eng Sci 49:4889–4895
12. Carrasco J, López-Durán D, Liu Z, Duchoň T, Evans J, Senanayake SD, Crumlin EJ, Matolín V, Rodríguez JA, Ganduglia-Pirovano MV (2015) Angew Chem Int Ed 54:3917–3921
13. Corral Valero M, Raybaud P, Sautet P (2006) J Phys Chem B 110:1759–1767
14. Miheţ M, Lazar M, Almăşan V (2009) J Phys: Conf Ser 182:012051
15. Valencia D, Peña L, Uc VH, García-Cruz I (2014) Appl Catal A 475:134–139
16. Lin K-H, Wang C-B, Chien S-H (2013) Int J Hydrog Energy 38:3226–3232
17. Melchor-Hernández C, Gómez-Cortés A, Díaz G (2013) Fuel 107:828–828
18. Han X, Yu Y, He H, Shan W (2013) Int J Hydrog Energy 38:10293–10304
19. Song H, Ozkan U (2009) J Catal 261:66–74
20. Soykal II, Sohn H, Ozkan US (2012) ACS Catal 2:2335–2335
21. Li Y, Zhang B, Tang X, Xu Y, Shen W (2006) Catal Comm 7:380–386
22. Lu Y, Li S, Guo L (2013) Fuel 103:193–199
23. Yu C, Hu J, Zhou W, Fan Q (2014) J Energy Chem 23:235–243
24. Zheng W, Zhang J, Ge Q, Xu H, Li W (2008) Appl Catal B 80:98–105
25. Osorio-Vargas P, Flores-González NA, Navarro RM, Fierro JLG, Campos CH, Reyes P (2015) Catal Today 259:27–38
26. Sánchez-Sánchez MC, Navarro RM, Fierro JLG (2007) Catal Today 129:336–345
27. Chiou JYZ, Siang J-Y, Yang S-Y, Ho K-F, Lee C-L, Yeh C-T, Wang C-B (2012) Int J Hydrog Energy 37:13667–13673
28. Sánchez-Sánchez M, Navarro R, Fierro J (2007) Int J Hydrog Energy 32:1462–1471
29. Cassinelli WH, Feio LSF, Araújo JCS, Hori CE, Noronha FB, Marques CMP, Bueno JMC (2007) Catal Lett 120:86–94
30. Mazumder J, de Lasa HI (2014) Catal Today 237:100–110
31. Mokhnachuk OV, Yaremov PS, Nauky P (2006) Theor Exp Chem 42:318–323
32. Juan-Juan J, Román-Martínez MC, Illán-Gómez MJ (2009) Appl Catal A 355:27–32
33. Luisetto I, Tuti S, Battocchio C, Lo Mastro S, Sodo A (2015) Appl Catal A 500:12–22
34. Dan M, Mihet M, Tasnadi-Asztalos Z, Imre-Lucaci A, Katona G, Lazar MD (2015) Fuel 147:260–268

35. Denis A, Grzegorczyk W, Gac W, Machocki A (2008) Catal Today 137:453–459
36. Li C, Chen Y-W (1995) Thermochim Acta 256:457–465
37. Zhang L, Wang X, Tan B, Ozkan US (2009) J Mol Catal A: Chem 297:26–34
38. Zhang S, Li L, Xue B, Chen J, Guan N, Zhang F (2006) React Kinet Catal Lett 89:81–87
39. Navarro RM, Álvarez-Galván MC, Rosa F, Fierro JLG (2006) Appl Catal A 297:60–72
40. Navarro RM, Guil-Lopez R, Ismail AA, Al-Sayari SA, Fierro JLG (2015) Catal Today 242(Part A):60–70
41. Koo KY, Roh H-S, Seo YT, Seo DJ, Yoon WL, Park SB (2008) Appl Catal A 340:183–190
42. Alvero R, Bernal A, Carrizosa I, Odriozola JA (1987) Inorg Chim Acta 140:45–47
43. Ledford JS, Houalla M, Proctor A, Hercules DM, Petrakist L (1989) J Phys Chem 26:6770–6777
44. Egelhoff WF (1987) Surf Sci Rept 6:253–415
45. Rodriguez JA, Campbell RA, Goodman W (1991) J Phys Chem 95:5716–5719
46. Ganduglia-Pirovano MV (2015) Catal Today 2:1–13
47. Jacobs G, Graham U, Chenu E, Patterson P, Dozier A, Davis B (2005) J Catal 229:499–512
48. Iriondo A, Barrio VL, Cambra JF, Arias PL, Guemez MB, Sanchez-Sanchez MC, Navarro RM, Fierro JLG (2010) Int J Hydrogen Energy 35:11622–11633
49. Sanchez-Sanchez MC, Navarro Yerga RM, Kondarides DI, Verykios XE, Fierro JLG (2010) J Phys Chem A 114:3873–3882
50. Jeon J, Yu BD, Hyun S (2015) Curr Appl Phys 15:679–682
51. Mohsenzadeh A, Bolton K, Richards T (2014) Surf Sci 627:1–10
52. Zhang M, Chen J, Yu Y, Zhang Y (2013) Appl Surf Sci 287:97–107